Surface & Coatings Technology 503 (2025) 131985

Contents lists available at ScienceDirect

Surface & Coatings Technology

journal homepage: www.elsevier.com/locate/sct

Full length article

Friction surfacing of aluminum alloys on Ti6Al4V - Investigation of process parameters, material deposition behavior and bonding mechanisms

Marius Hoffmann [a,*], Arne Roos [a], Benjamin Klusemann [a,b]

[a] Helmholtz-Zentrum Hereon, Institute of Material and Process Design, Solid State Materials Processing, Max–Planck-Straße 1, 21502 Geesthacht, Germany
[b] Leuphana University Lüneburg, Institute for Production Technology and Systems, Universitätsallee 1, 21335 Lüneburg, Germany

ARTICLE INFO

Keywords:
Friction surfacing
Dissimilar aluminum–titanium joining
Material deposition theory
Bonding mechanism
Diffusion

ABSTRACT

This study addresses a detailed investigation of friction surfacing (FS) process parameters for two materials with low metallurgical compatibility, i.e. Al and Ti, to achieve successful depositions, representing a very challenging task. The difference in suitable process parameters between two Al alloys onto Ti is highlighted. For instance, AA6082 requires higher rotational speeds than AA7050, resulting in higher process temperatures that lead to the formation of intermetallics with a thickness of about 0.3 μm at the interface. This indicates that diffusion is the main bonding mechanism for AA6082, while mainly mechanical interlocking contributes to bonding for AA7050. Additionally, AA6082 presents slightly thicker (~240 μm) and wider (~28 mm) layers than AA7050 (~185 μm and ~24 mm, respectively). Based on the experimental results, a new theory of material deposition is proposed for the dissimilar Al/Ti material combination, as a unique deposition behavior could be identified. The experiments show that material is deposited only in the peripheral areas of the stud, but not in the center, as typically seen in FS. Higher local process temperatures in the peripheral areas result in lower local flow stresses, which increase stud shearing and thus deposition of the plasticized stud material.

1. Introduction

Solid state joining processes allow the bonding of materials below their melting temperatures. One process for coating in solid state is friction surfacing (FS), which was first mentioned by Klopstock and Neelands [1]. During the FS process, a consumable stud material is deposited on a substrate material. First, the stud material starts rotating until its desired rotational speed is reached. Afterwards, an axial movement towards the substrate is introduced. Once the materials touch, friction between the tip of the stud and the substrate surface leads to frictional heat and the stud tip starts to plasticize, whereas the heat generation and the temperature increases. The stud tip starts to deform plastically and the heat generation shifts from solid friction to viscous shearing between the stud tip and the already deposited material. Superimposing a translational movement between the stud and substrate material enables the deposition of stud material layers onto the substrate. The process ends with the retraction of the stud material from the substrate plate once the stud material is consumed or the desired length of the layer is reached. The whole process takes place in solid state, i.e. no global melting occurs, whereas the plasticized material is bonded to the substrate by diffusion processes and mechanical interlocking. This leads to a variety of similar material combinations that can be joined together, e.g. steels [2] or aluminum alloys [3]. Dissimilar material combinations, e.g. aluminum on steel [4], or various other stud materials on non-ferrous substrates [5] can also be joined. FS applications range from wear resistance improvement [6] by adding powdered SiC particles to AA6082 stud material as well as using AA2024-Al_3NiCu studs [7]. Furthermore, FS enables the improvement of corrosion behavior for aluminum deposits [8]. Agiwal et al. [9] demonstrated the use of FS as crack repair method. In addition, the application of multiple layers on top of each other enables its use as an additive manufacturing process as shown for AA2014 [10], for AA2024 [11,12] or for 304L stainless steel [13].

Dissimilar material combinations containing aluminum have a broad range of applications, such as railways, aeronautics, and defense [14]. In the automobile and aerospace industry, aluminum and titanium alloys belong to the most frequently used metallic materials [15]. Joining these two metals results in structures combining the advantages of both materials, i.e. lightweight, corrosion-resistant and high-strength. However, joining such chemically and physically vastly different materials is challenging. For instance, fusion-based welding processes lead, among other possible welding defects, to brittle intermetallic compounds (IMC) at the joint interface as observed for laser beam welding of AA6056 to Ti6Al4V by Vaidya et al. [16], as

* Corresponding author.
E-mail address: marius.hoffmann@hereon.de (M. Hoffmann).

https://doi.org/10.1016/j.surfcoat.2025.131985
Received 27 September 2024; Received in revised form 7 February 2025; Accepted 26 February 2025
Available online 7 March 2025

a high energy input is required to melt the joining partners [17]. In contrast, for solid state joining processes, e.g. friction stir welding (FSW) or friction stir spot welding (FSSW), the characteristically lower heat input makes them promising candidates for joining such dissimilar material combinations due to generally not being susceptible for build up of IMCs [18] and realizing mechanical and chemical bonding [19]. The formation of IMC layer requires less activation energy due to introduction of severe plastic deformation as shown by Kar et al. [20] for FSW of AA1900 to Ti Grade 2. In addition, as shown in the study of Kim and Fuji [21] for post friction welded heat treatments, an IMC thickness of 5 μm can contribute to the bonding properties of the joint. The majority of published papers focusses on aluminum alloys providing a solidus temperature above 500 °C in order to allow high energy inputs during the joining process. High energy inputs result in high process temperatures that are necessary to form IMCs, which contribute to bonding and joint strength according to Aonuma and Nakata [22]. Kar et al. [23] showed also that by changing the tool offset to the Ti side, the degree of deformation of the Ti side of the FSW weld affects the development of IMC.

Single or multiple Al layers on dissimilar materials, e.g. Ti substrates, can be used as buffer layers for other joining processes, e.g. fusion welding to reduce IMC at the interface, or as assisting processes for other solid state joining processes such as FSW as described by Huang et al. [24] and Zhou et al. [25] for Al–Ti and Al-Steel, respectively. Instead of pure titanium components, hybrid Al–Ti components that require good corrosion resistance or high mechanical properties locally can be fabricated in this way, reducing the amount of Ti used and thus component cost.

With regard to FS, there is very little literature on aluminum-titanium material combinations. Rao et al. [5] attempted to deposit AA6063 on Ti6Al4V but failed because mainly flash was formed instead of a layer. Esther et al. [26] successfully deposited 4.1 to 11.5 mm thick layers of AA2124 stud material, containing 4 wt.% of B4C particles on Ti6Al4V substrates, detecting no IMCs at the interface. The high layer thicknesses are justified by the authors as a result of the low deposition speed and high axial force, i.e. 0.25 mm/s and 30 kN, respectively. On the other hand, Huang et al. [24] achieved an average layer thickness of 0.23 mm of AA6082 on Ti6Al4V using the process parameters 1.5 mm/s and 3.0 kN. After FS process, an Al-sheet was joined onto the deposited layer using FSW to improve the joint efficiency of the dissimilar Ti/Al joints. Afterwards, nanometer-sized IMCs were detected at the Ti-Al interface via transmission-electron microscopy (TEM). A similar finding was reported by Reddy et al. [27] for depositing the metal matrix composite AA2124-SiCp on Ti6Al4V.

Furthermore, the material flow and deposition behavior during the FS process is not completely understood although a lot of research has been published regarding this topic. Fukakusa [28] used tracer material inside the studs to study the material flow, whereas the tracer material in the studs' center formed the layer. The surrounding material covered the tracer material and formed the flash. Furthermore, Fukakusa introduced the term 'real rotational contact plane'. This term describes the zone around the stud materials' rotational axis from where material is deposited to the substrate. A similar approach was pursued by Hoffmann et al. [29] to investigate the layer formation mechanisms for AA2024 and AA5083 by tracking the path of the stud material to its position in the layer. This was achieved by using different inner and outer stud materials. It was identified that the material from the center of the stud forms the center of the layer, whereas the material in the bottom, on the advancing side (AS) and in the top of the layer is formed by material from the stud periphery. The top part of the layer is formed at the rear edge of the stud, where the material mainly shears off, indicated by a strong shear texture. Experiments using powder based marker material inside the stud to visualize material flow during FS were carried out by Rafi et al. [30] and Belei et al. [31]. According to the findings of Rafi et al. [30], the material flows from AS over the retreating side (RS) to the center. Based on the particle distribution in the deposits, Belei et al. [31] concluded that the material flow predominantely occurs parallel to the substrate surface pointing to torsional shear flow. Some research also addressed the stud tip appearance after the FS process as an indicator for the material flow. Liu et al. [32] detected a concavity at the stud tip in the studs' center, which they explained as an indicator of energy concentration in this region. However, Rafi et al. [33] stated that this concavity might be the result of a vortex generation that leads to an upward flow at the center of the stud. Depositing commercially pure Cu on low carbon steel by Rao et al. [34], a smooth surface at the stud tip after the process was identified as an indicator for an unsuccessful deposit, where a rough stud tip surface indicated a successful material deposition. The same phenomena were observed by da Silva et al. [35] depositing aluminum on low carbon steel.

Due to the very different material properties and the low metallurgical compatibility of Al and Ti, a successful deposition is challenging. The present study investigates the process parameters for Al–Ti FS using two different Al alloys, AA6082 and AA7050. For AA6082, a single process parameter set, enabling successful deposition, was already reported by Huang et al. [24], whereas no literature for FS of AA7050 to Ti6Al4V, albeit it is a material combination of great interest in the aerospace industry for the development of hybrid parts, could be found. Therefore, both material combinations were used to potentially identify parameter ranges that enable successful deposition of homogeneous layers. Additionally, the study attempts to reveal the bonding mechanisms during FS of Al to Ti and discusses them as a function of the Al alloy used and the process temperatures reached. Furthermore, the material deposition behavior during FS for the dissimilar material combination of Al to Ti alloys was investigated. This study shows that this behavior differs from what has been suggested in the literature for material combinations where stud and substrate material have more similar material properties. At first, a parameter study was carried out to achieve successful depositions. Then, the influence of the process parameters on the deposition behavior was investigated in order to derive a hypothesis on how material deposition occurs during the process. Via microstructural analyzes the interface was investigated regarding bonding mechanisms and IMC formation.

2. Materials and methods

In this work, AA6082-T6 and AA7050-T651 rods were used as stud material. The rods were machined to the dimensions 20 mm (diameter) × 125 mm (length). Their chemical compositions are listed in Table 1. As the substrate material, 3 mm thick Ti6Al4V sheets (250 mm long and 100 mm wide) were selected, see chemical composition in Table 2. The substrate has been ground using 150 grid SiC paper in order to remove any oxide layers on its surface. Additionally, an 8 mm thick AA2024-T3 backing plate was employed, relevant in terms of heat conduction conditions. The experiments were made on a specially designed friction surfacing machine (Henry Loitz Robotik, Germany), allowing process forces up to 60 kN, rotational speeds up to 6000 rpm and a maximum torque of 200 N m. During deposition, process forces and displacements in x-, y-, and z-direction, as well as rotational speed and spindle torque were recorded. For the stop action experiments, the stud rotational and translational movement were stopped in the steady state region after 100 mm deposition length and the subsequent retraction of the stud was disabled.

For the temperature measurements, holes of 0.6 mm diameter were drilled from the bottom of the substrate until 0.5 mm to the substrate surface. The holes have been placed 5 mm equidistant and orthogonal to the deposition direction for measuring the temperature on the AS, center and RS, see Fig. 1. Therefore, the distribution of the thermocouples allows the analysis of a process temperature profile across the layer width. The deposition starts 60 mm in front of the thermocouple positions and stops 90 mm behind them, resulting in a total deposition length of 150 mm. Type K thermocouples were

Table 1
Chemical composition in wt.% for AA6082 and AA7050 according to DIN EN 573-3 [36].

Alloy	Si	Fe	Cu	Mn	Mg	Cr	Zn	Ti	Zr	Al
AA 6082	0.7–1.3	0.5	0.1	0.4–1.0	0.6–1.2	0.25	0.2	0.1	–	bal.
AA 7050	0.12	0.12	2.0–2.6	0.1	1.9–2.6	0.04	5.7–6.7	0.06	0.08–0.15	bal.

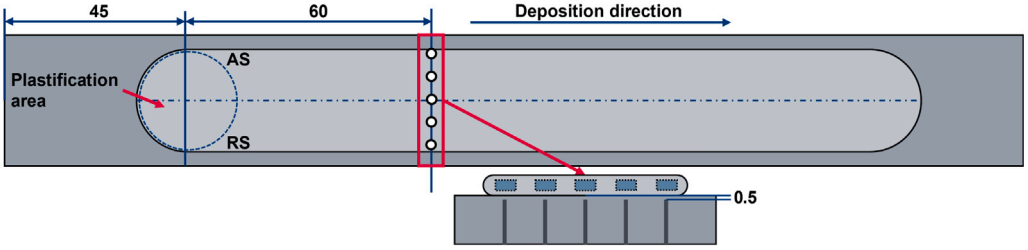

Fig. 1. Schematic of resulting FS deposit, including thermocouple and EBSD scan positions. All dimensions in mm.

Table 2
Chemical composition in wt.% for Ti6Al4V according to ASTM B265 [37].

Alloy	Fe	C	N	H	O	Al	V	Ti
Ti6Al4V	≤0.4	≤0.08	≤0.05	≤0.015	≤0.2	5.5–6.75	3.5–4.5	bal.

mounted, recording the temperatures at a frequency of 50 Hz. For subsequent process temperature analysis, the threshold temperature was set to 40 °C, i.e. once the temperature exceeds this value, the time is set to 0 s. For the microstructural analyses, the deposits were cut, ground and polished using an Axitom cutting machine and a Tegramin-20 grinding and polishing machine (Struers, Denmark), respectively. Specimens were plane ground for 2 min using SiC abrasive paper with a grit size of 320 µm, followed by 6 min of fine grinding and polishing with 9 µm and 1 µm diamond suspension, respectively. Oxide polishing was performed using colloidal silica suspension for 8 min. Optical analysis was performed with a VHX-6000 digital microscope (Keyence, Germany). The steady state layer thickness was measured at five positions across the entire layer width and then averaged. The stud tip geometry after the process was measured using a caliper. For further investigation of the sample interfaces, the scanning electron microscope Quanta 650 FEG (Thermo Fisher Scientific Inc., USA) equipped with an EDAX Octan Elect Super energy-dispersive X-ray spectroscopy (EDS) system (AMETEK Inc., USA) was used. The EDS line scans consist of 1024 points and a total length of 2 µm. The microstructure was analyzed using an EDAX Velocity series electron backscatter diffraction (EBSD) detector (AMETEK Inc., USA), applying as scan parameters a step size of 0.2 µm, a working distance of 17 mm and a voltage of 15 kV. A total of five scans were performed for each alloy, i.e. in the center and at ±5 mm and ±10 mm on AS and RS, as indicated in Fig. 1. The EBSD data was analyzed using MTEX toolbox version 5.8.1 in MATLAB (The Mathworks Inc., USA) selecting a misorientation threshold of 2° to define grain boundaries, i.e. low-angle grain boundaries, as well as a minimal grain size of 3 pixels. Misorientations greater than 15° are referred to as high-angle grain boundaries.

3. Results

3.1. Process parameter range and deposit appearance

For the process parameter development, the three main process parameters, i.e. axial force, rotational speed and traverse speed, were investigated experimentally to achieve a consistent and homogeneous deposit. The deposits were considered homogeneous if two conditions were met: The layer is continuous across the main bonding width (BW) as well as in the steady state deposition area (DA). The main bonding width (BW) is the defect free width measured between the unbonded

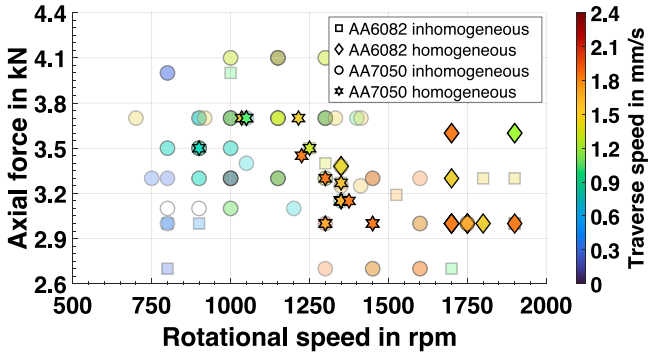

Fig. 2. Process parameter investigation of AA6082 and AA7050 on Ti6Al4V. The deposits are characterized according to their homogeneous or inhomogeneous deposition appearance.

AS and RS areas of a deposited layer. In the transition area (TA), the stud is accelerated from the plasticizing zone (PA) to the translational deposition speed in the steady state deposition area (DA). Continuous means that the layer surface shows no gaps through which the substrate is visible. Inhomogeneous deposits show irregularities in areas in the DA along the BW of the layer where no material is deposited on the substrate. The process parameters were identical for both the plastification and deposition phase. The investigated parameter range is indicated in Fig. 2. Homogeneous deposits can be achieved either by high rotational speeds at low axial forces or vice versa for a specific traverse speed. The two alloys AA6082 and AA7050 can be clearly distinguished by successful deposition based on the different rotational speeds, where lower rotational speeds are needed for AA7050. In terms of axial forces, the range was similar for both alloys, i.e. between 3.0 and 3.7 kN.

Overall, the FS process parameters for achieving homogeneous deposits must be carefully selected to match the energy input required for proper material flow and bonding, based on the initial parameters from Huang et al. [24]. However, the study shows that even small variations in these parameters can lead to significant changes in deposition quality for Al on Ti substrates, as noted by Rao et al. [5]. Given the challenges observed, future research might explore broader parameter ranges to establish more robust windows for industrial applications, possibly through systematic design of experiments and additional support by advanced process modeling. Nonetheless, it is noticeable that the resulting parameter range for homogeneous deposits is narrow compared to parameter investigations of other material combinations such as similar Ti6Al4V by Fitseva et al. [38] or dissimilar AA6082-AA2024 by Gandra et al. [39].

For in-depth analyses, three parameter combinations were selected, which are listed in Table 3. The identical parameter sets 1 and 2 are

Table 3
FS process parameters used for in-depth investigations and resulting measured variables during the process.

Set	Alloy	Axial force [kN]	Rotational speed [rpm]	Traverse speed [mm/s]	Spindle torque [N m]	Stud consumption rate [mm/s]	Maximum process temperature [°C]
1	AA 6082	3	1750	1.65	10.69 ± 0.96	0.34 ± 0.01	495.0 ± 6.8
2	AA 7050	3	1750	1.65	9.35 ± 1.42	0.17 ± 0.01	399.0
3	AA 7050	3.15	1350	1.62	10.57 ± 0.57	0.12 ± 0.01	428.2 ± 6.5

used to compare the process behavior and temperatures of AA6082 and AA7050, where this leads to a homogeneous appearance for AA6082 and an inhomogeneous appearance for AA7050. The improved process parameter combination for AA7050, leading to a homogeneous deposition appearance for this alloy, represents parameter set 3. The deposition appearances and the corresponding stud tips are shown in Fig. 3. The homogeneous appearances of AA6082 and AA7050 deposits show a continuous FS-typical surface structure, whereas the inhomogeneous AA7050 deposit, deposited via process parameter set 2, contains gaps where no material is deposited to the substrate. For AA6082, the material deposition starts in the transition area at approximately 25 mm of the deposition length, indicating an insufficient plastification phase, i.e. not enough heat was generated until this point.[1] For the homogeneous deposits, Fig. 3(a, c), at the position of stud retraction a keyhole like surface appearance is visible. Within this region, material is no longer deposited to the substrate. Furthermore, the surface area of the stud tip can be subdivided in two sections. The inner section close to the rotational axis is the counterpart of the keyhole, see Fig. 3(a, c). It has a smoother surface and protrudes from the rest of the stud tip area. Additionally, the outer section has a rougher surface appearance. Similar surface appearance was observed by Li et al. [40] for dissimilar FS of AA5083 on DH36 steel. The depositions of Sahoo et al. [41,42], depositing AA6063 over IS 2062 low carbon steel and AISI 316 stainless steel respectively, show a keyhole like surface at stud retraction position as well.

Using parameter set 1 compared to set 2 leads to a higher stud consumption rate for AA6082 (0.34 mm/s) than AA7050 (0.17 mm/s). For the parameter set 3, the consumption rate of AA7050 is even lower (0.12 mm/s). For AA6082, a higher average spindle torque during the process is measured, i.e. 10.69 N m, whereas the spindle torque for AA7050 studs was 3.35 N m (set 2) and 10.57 N m (set 3), respectively. Therefore, when applying the same process parameters, a higher process energy input is achieved for AA6082 (set 1) than for AA7050 (set 2) leading to higher process temperatures, see Section 3.3.

3.2. Microstructure

In terms of microstructural analysis, the layers were cut perpendicular to the deposition direction, Fig. 4. Fig. 4(a–b) show the macrographic cross-sections for the AA6082 (set 1) and AA7050 layers (set 3). For the AA6082 deposit, the average layer thickness is 240.2 ± 59.8 µm, whereas the layer width and bonded layer width is 28.24 mm and 27.61 mm, respectively. The layer geometries are summarized in Table 4. The micrograph of AA6082-Ti6Al4V, Fig. 4(c, e), shows the interface, which reveals a non-continuous IMC layer with a maximum thickness of approximately 0.3 µm. The EDS linescan in Fig. 4(g) shows a small concentration plateau close to the interface, a decrease of Al-concentration from 82 to 62% on the Al-side and an increase of Ti and Mn to 10% and 7%, respectively. The concentration of Mn is increased in the IMC region and significantly higher than in the AA6082 base material as well as on the Ti-side. The thickest IMC layer was detected in the center of the deposit. The thickness of the layer is not uniform and decreases towards the edge of the layer, where no IMC layer can be detected using SEM, see Appendix A - Interface AA6082-Ti6Al4V. At the AA7050-Ti6Al4V interface, no evidence of intermetallic phases was detected, see Fig. 4(d,f,h). Appendix B - Interface AA7050-Ti6Al4V shows parts of the interface investigation for AA7050 on Ti6Al4V for the sake of completeness, where mechanical interlocking was identified. A discussion about the bonding mechanisms is provided in Appendix C - Bonding mechanisms.

[1] By increasing the rotational speed or the plastification time this region could be minimized, however, for consistency the process parameters between plastification and deposition phase were chosen constant within this study.

Table 4
Layer geometries of the homogeneous deposits.

Set	Thickness [µm]	Width [mm]	Bonded width [mm]
1	240.2 ± 59.8	28.24	27.61
3	184.7 ± 41.5	23.78	21.66

The EBSD results, i.e. inverse pole figure maps and pole figures, are displayed in Fig. 5. Each scan has a height of about 140 µm and thus covers more than 50% of the layer's height. The average grain sizes for the two alloys are in the range between 2.01 and 2.78 µm (AA6082) and 1.40 and 1.95 µm (AA7050). The {110} and {111} pole figures below the inverse pole figure maps present $B\{\bar{1}12\}\langle 110\rangle$ and $\bar{B}\{1\bar{1}2\}\langle\bar{1}\bar{1}0\rangle$ shear texture components in the center of the layer, which indicates that the stud material might be sheared off at the rear edge of the studs [29]. In the AA7050 layer, the shear texture is only present in the center of the layer, whereas in the AA6082 layer, which will be discussed later, it is present across the entire layer width.

3.3. Temperature measurement

Fig. 6 shows the FS process temperatures measured in the substrate at 0.5 mm distance to the interface in the center of the deposit and at 5 mm on AS and RS. For all parameter sets, the maximum temperature was measured in the center of the deposition, where AA6082 (490.3 °C) shows an approximately 60 to 90 K higher maximum temperature compared to AA7050. The maximum temperature for AA7050 deposition using parameter set 3 is higher (422.9 °C) than the temperature measured for set 2, which indicates that a sufficient high deposition temperature needs to be reached to obtain a homogeneous deposition. Table 3 gives the average values of the measured maximum temperatures of three processes. Considering the solidus temperatures of AA6082 and AA7050 of 606 °C and 488 °C, respectively [43], the maximum process temperatures are between 87 and 92% of the solidus temperatures of the stud materials.

For both materials, a drop in process temperature at the deposits center was measured. This drop occurs when the stud center reaches the position of the thermocouple. Therefore, the temperature measurements indicate that the highest temperature is not in the studs' center but somewhere between its center and its maximum radius leading to a M-shaped temperature profile, measured within this study along the deposition path axis in the deposit center, i.e. in longitudinal direction. Perpendicular to this direction, i.e. in traverse direction, a similar shape is expected based on the fact that the temperatures on AS and RS are higher compared to the center when the drop of temperature is detected, which agrees with the results of numerical simulations [44].

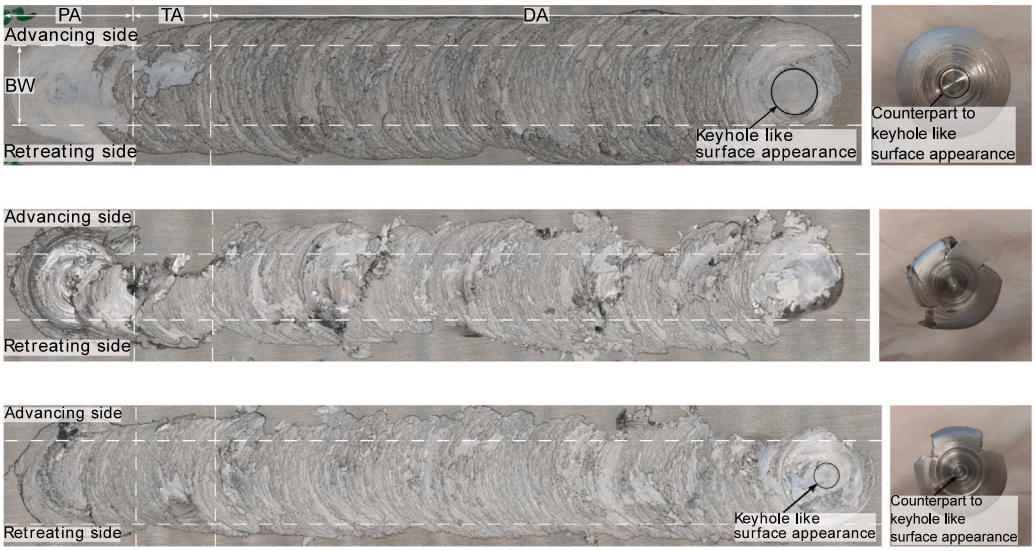

Fig. 3. Deposit and corresponding stud tip appearances of the process parameters investigated: (a) homogeneous AA6082 deposit - set 1, (b) inhomogeneous AA7050 deposit - set 2, (c) homogeneous AA7050 deposit - set 3. All layers are divided into the following areas: PA - plastification area, TA - transition area, DA - deposition area. The corresponding bonding width is denoted as BW.

3.4. Stop action tests

Stop action tests were conducted to get a better understanding of the material deposition behavior during the FS process. Fig. 7(a) shows the cross section in transverse direction. Two different zones can be distinguished. In the deposits' center, the first zone, no deposition seems to take place, where the material close to the rotational axis of the stud is in direct contact to the substrate surface but no shear layer can be identified. On both AS and RS, i.e. in the peripheral region of the stud, a thin material layer is deposited to the substrate, representing the second characteristic zone. In this zone shearing occurs. Similar observations are made in Fig. 7(b) along the longitudinal section. In front of the studs' center, material is deposited to the substrate. However, behind the studs' center, there is a significant gap in deposition direction, which can be defined as another zone. This gap is an indicator that material in the middle of the layer is being removed by the protruding material in the center of the stud during the translational movement. The different stud zones observed in the stop action tests coincide with the stud tip surface and layer keyhole appearance mentioned in Section 3.1.

4. Discussion

4.1. Process parameter window with regard to different alloys

One factor that determines the size of the process parameter window is the diffusion rate, which is lower for diffusion between Al and Ti compared to other material combinations, e.g. Al-Al or Al-steel, and therefore requires higher process temperatures to increase the diffusion rate and achieve good bonding during the relatively short FS processing times (~10 to 20 s). Al alloys have solidus temperatures below 610 °C, which limits the possible deposition temperatures. Therefore, the range of FS process parameters is limited to the corresponding energy inputs required to reach these temperatures.

As shown in Fig. 2, higher rotational speeds are required to achieve a homogeneous deposit for the deposition of AA6082 compared to AA7050. One reason for this is the difference in the thermal conductivity, which is 170 W/(m K) and 153 W/(m K) for AA6082 [45] and AA7050 [46], respectively. The higher thermal conductivity of AA6082 leads to a faster heat conduction to the colder stud material. Therefore higher rotational speeds are required to maintain a sufficient process temperature at the stud tip. Another aspect is the mechanical behavior at high temperatures. Reimann [47] showed in his work on refill FSSW that AA7xxx alloys exhibit significant lower flow stresses at higher temperatures than AA6xxx alloys under the same processing conditions, indicating a lower resistance to rotational movement. In addition to the higher rotational speeds that are required to achieve sufficient plastic deformation, this also leads to higher process torque for AA6082 compared to AA7050. In turn, this implies a higher energy input, leading to higher process temperatures for AA6082, which are required to deposit AA6082 successfully, consistent with the performed process temperature measurements in this work.

Comparison of homogeneous and inhomogeneous AA7050 deposits showed that the homogeneous deposit is obtained for parameter set 3 at a higher process temperature. However, the rotational speed for parameter set 2, leading to an inhomogeneous deposition, was higher, which should lead to a higher process temperature. An explanation for that might be that the higher rotational speed results in too much heat generation, which, through the lower flow stress, leads to excessive softening of the stud tip material. This softer material will be pushed out of the process zone underneath the stud tip immediately by the colder, harder stud material. Therefore the hotter stud material stays within the process zone for a shorter amount of time, also indicated by the higher axial feed rate for parameter set 2. As a result, more stud material is fed, i.e. the machine control increases the axial feed rate of the stud in order to maintain the specified process force. However, because the warm stud material is sheared off the stud tip too quickly, colder, firmer material is subsequently in contact with the substrate, which results in an increase in the process force. If this process is repeated over the entire process time, it results in an instable process, an inhomogeneous deposition behavior and, due to the inertia of the measurement system, to constantly lower measured temperatures. In addition, the measured spindle torque during the process is an indicator of stick/slip. Set 3 obtains a higher spindle torque (9.49 N m) as set 2 (8.04 N m), Table 3. Higher spindle torques indicate stronger adhesion (sticking) of the stud material to the substrate. Sticking increases the plastic deformation and thus the process temperature.

Overall, the behavior depends on the resulting energy input. By selecting the process parameters accordingly, the energy input is kept below the threshold for inhomogeneous deposition behavior due to

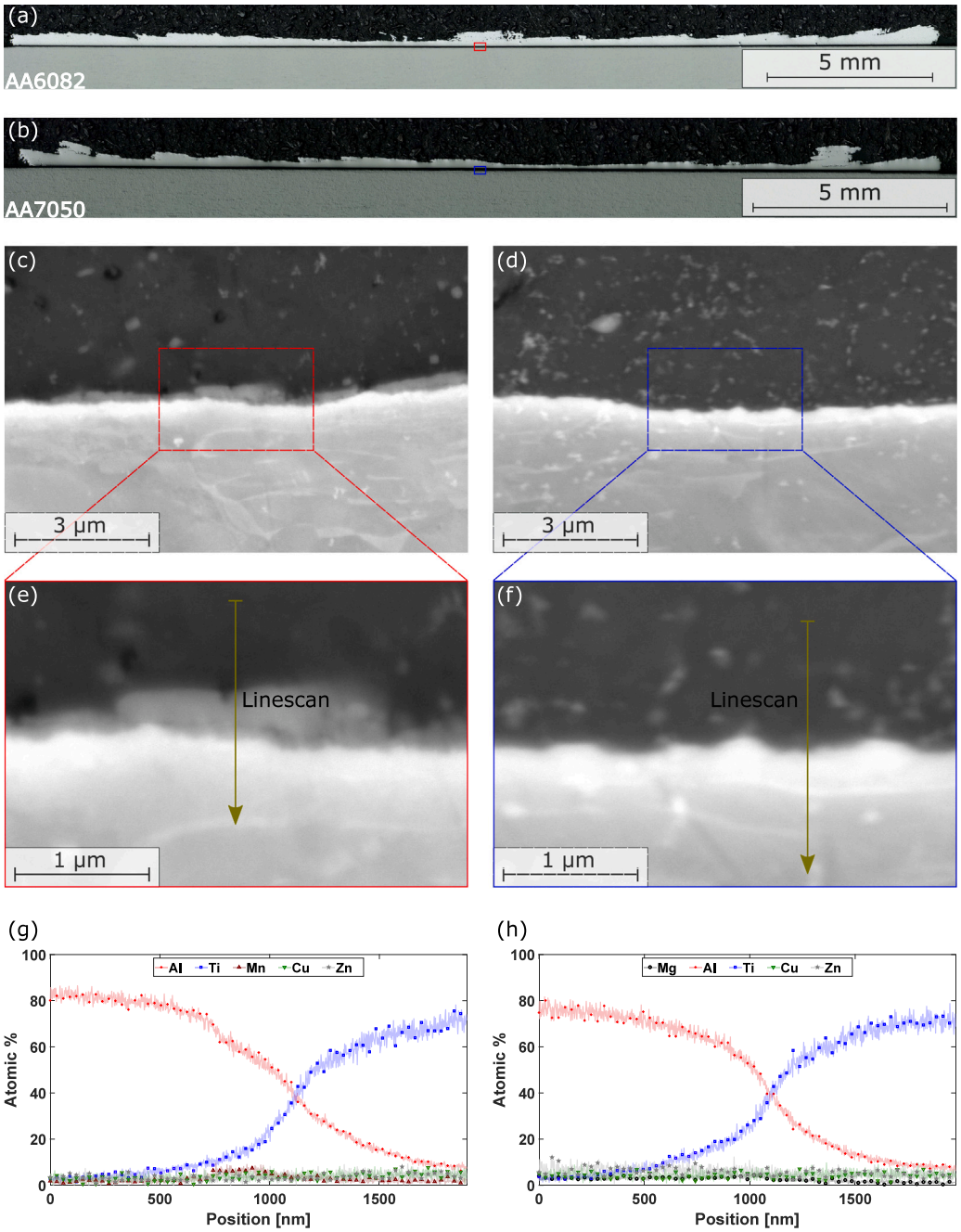

Fig. 4. Macrographs of cross section (a,b), macrographs of interface at a magnification of 20,000×(c,d), and at 60,000×(e,f) as well as EDS linescan (g,h) in homogeneous deposits of AA6082 (set 1) and AA7050 (set 3) on Ti6Al4V.

excessive stud softening. However, when the process parameters axial force or rotational speed are selected too low, the generated heat is not sufficient enough to ensure necessary process temperatures for a complete plastification of the stud material, which does not bond to the substrate and results in no or inhomogeneous deposition.

4.2. Strain rate sensitivity, flow stress and microstructure

In this study, notable differences in the friction surfacing behavior of AA6082-T6 and AA7050-T651 on Ti6Al4V substrates have been observed. These variations can be attributed to the distinct mechanical and microstructural properties of these alloys under the high strain rates and temperatures encountered in friction surfacing. According to Djapic Oosterkamp et al. [48], AA6082 exhibits a unique strain rate sensitivity that decreases at higher rates, leading to potential shear banding or deformation bands. This behavior was reproduced in the experiments where AA6082 required higher rotational speeds (resulting in higher process temperatures) for successful deposition. The peak temperatures measured for AA6082 were approximately 495 °C, which is consistent with the necessity for increased energy input to overcome its higher flow stress, particularly at the strain rates experienced during friction surfacing (estimated from the torque and rotational speeds measured). In contrast, AA7050, as described by Li et al. [49], demonstrates a more consistent increase in flow stress with strain rate, albeit at a lower rate of flow stress increase than AA6082, suggesting

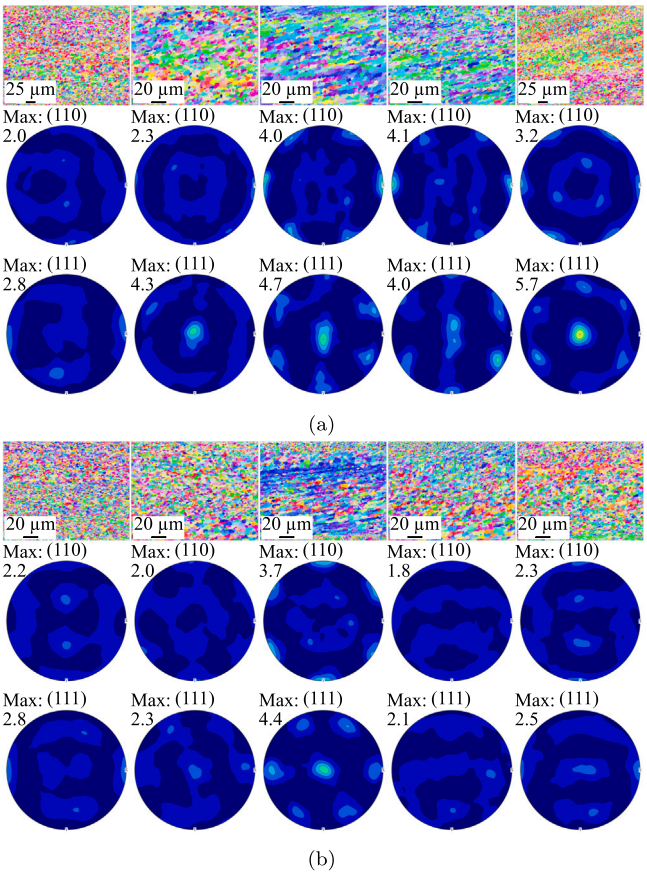

Fig. 5. EBSD results: inverse pol figure maps and pole figures of AA6082 - set 1 (a) and AA7050 - set 3 (b).

that a reduced energy input is required for plasticization. This is supported by the findings where AA7050 reached a maximum temperature of approximately 428 °C for successful deposition, indicating to the lower thermal requirements. The microstructural analysis by Schikorra et al. [50] on AA6082 during extrusion, showing grain elongation and significant deformation in shear-intensive zones, corresponds with the FS observations. The EBSD results from this study indicate a stronger shear texture across full layer width in AA6082 deposits, suggesting that the material undergoes considerable shear-driven recrystallization during deposition, which is consistent with its dynamic recrystallization behavior noted by Krumphals et al. [51]. Shear texture was observed solely in the center of the AA7050 layer, contributing to its finer grain size (between 1.40 and 1.95 µm) compared to AA6082 (between 2.01 and 2.78 µm). However, AA6082, requiring higher temperatures for deposition, resulted in thicker (240 µm) and wider (28 mm) layers compared to AA7050 (185 µm thick, 24 mm wide), possibly due to AA6082's different flow stress and response to the given FS process conditions. On the other hand, AA7050 (i.e. due to recovery which can lead to grain boundary migration and subgrain formation without complete nucleation of new grains) shows less pronounced recrystallization due to its composition, which might also influence the bonding mechanism. The absence of IMCs in the AA7050-Ti6Al4V interfaces suggests that the bonding mechanism is dominated by mechanical interlocking, possibly due to lower temperatures reducing diffusion rates, supported by the temperature measurements mentioned above.

The formation of IMCs at the AA6082-Ti6Al4V interface, with a thickness of approximately 0.3 µm, indicates that diffusion plays a significant role in bonding for AA6082 under the given FS process conditions. This is directly linked to the higher process temperatures achieved with AA6082, enhancing atomic mobility at the interface. The lack of IMCs in AA7050 interfaces corresponds with the temperature data, suggesting insufficient thermal energy for significant diffusion. Instead, mechanical interlocking is apparently the dominant bonding mechanism, influenced by the alloy's different flow stress behavior and microstructural stability under the given process conditions. By integrating these findings with the experimental data, it can be determined how the inherent material properties of AA6082 and AA7050 affect their performance in friction surfacing. The higher thermal and energy (i.e. slightly higher torque times the higher rotational speed input required for AA6082 results in different deposition behavior, layer characteristics and bonding mechanisms compared to AA7050. This analysis not only explains the observed differences, but also offers insight into future parameter optimization for FS of dissimilar materials.

4.3. Material deposition theory

There have been few publications on theories of FS material deposition. In all these theories, material is deposited to the substrate from the center of the stud material in the 'real rotational contact plane' named by Fukakusa [28], leaving a concave stud tip after the process. As shown in the review by Gandra et al. [52], the stud material shears off from the stud tip in a shear plane between stud tip and already deposited material. The radius of the 'real rotational contact plane' is calculated using the following equation [28]:

$$r_c = \sqrt{\frac{d \cdot w \cdot v}{\pi \cdot v_{cr}}}, \tag{1}$$

where d is the layer thickness, w the layer width, v the traverse speed and v_{cr} the average stud consumption rate during the deposition process. This calculation is made under the assumption that the volumetric deposition rate, i.e. the deposited volume, is equal to the volumetric rod consumption rate, i.e. the consumed stud material. For a perfect deposition, r_c would be equal to the stud radius. However, since material is lost in the flash, r_c is less than the actual stud radius.

Therefore, the present findings, as well as also seen in other studies in literature dealing with dissimilar material combinations, e.g. [40], the assumption about the deposition behavior from similar material combinations cannot be transfered to dissimilar material combinations, at least if the difference in physical properties is rather huge. Most studies reporting unsuccessful material deposition like da Silva et al. [35] for AA6351 studs on 1020 carbon steel substrate or a smooth stud tip after the process by Rao et al. [34] when depositing Cu on steel, have in common that the material combination used is dissimilar, e.g. stud material is softer, has a higher thermal conductivity as well as a lower solidus temperature than the substrate material, thus making them metallurgical incompatible materials. Therefore, a material deposition theory is proposed in the following that can be applied not only for the dissimilar FS of Al to Ti alloys but also to other material combinations where stud and substrate material significantly differ in the aforementioned properties.

Despite the observation of different material deposition theories for similar and dissimilar material combinations, the temperature evolution during the FS process is expected to be the same for similar and dissimilar material combinations. The process temperature measurements within this study showed that the material at the studs' center axis has a lower temperature than the material in the peripheral regions, which is in agreement with the simulations of Zhang et al. [44] for Ti6Al4V or Kallien et al. [53] for AA5083 on AA7050. Near the center axis of the stud, the circumferential speed and thus the relative speed approaches zero, i.e. heat is generated mainly by plastic deformation and only to a small extent by friction. However, the highest temperature is not present at the outer circumference of the stud, see Fig. 6, which is in agreement with other studies, e.g. the temperature

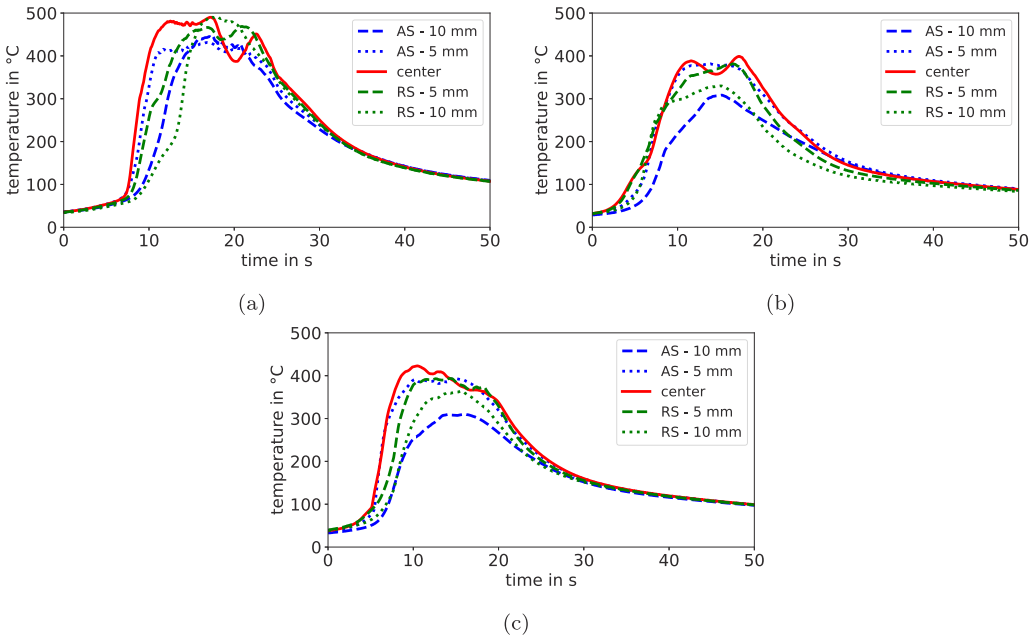

Fig. 6. Measured substrate temperatures during the process in the center and at 5 mm on AS and RS for AA6082 - set 1 (a), AA7050 - set 2 (b) and AA7050 - set 3 (c).

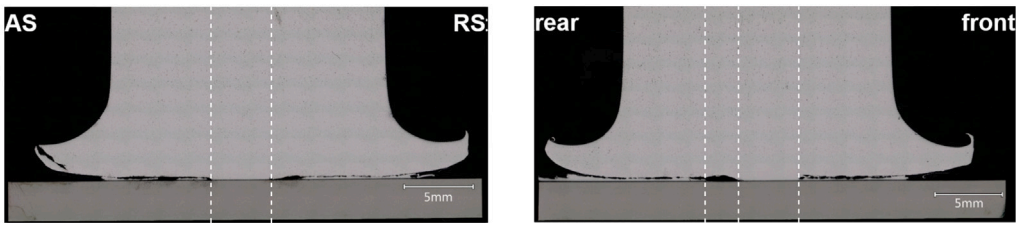

Fig. 7. Cross sections of the AA7050 (set 3) studs after stop action tests in transverse (a) and longitudinal direction (b). The white dashed lines mark the transition between the zones.

investigation of AA5083 on AA7050 by Kallien et al. [54]. In the outer stud circumference, local force conditions at the stud-substrate interface differ, i.e. local axial forces are lower, which decreases the heat generation by friction and plastic deformation. Both, the temperature and strain rate at the stud tip have an influence on the local shear flow stress σ_f of the stud material, i.e. flow stress decreases with increasing temperature and decreasing strain rate [55,56]. The radial strain rate profile of the stud material during the FS process is not investigated experimentally in literature yet but often estimated as constant within the whole deposit [57]. Pirhayati et al. [58] showed via numerical simulations that the strain rate in the deposit near the substrate interface does not change significantly with increasing radius r, however, at the top of the deposit, the strain rate profile increases with increasing r up to a certain value, followed by a strain rate decrease in the outer circumference region. Since the layer thickness in this work is very narrow, the behavior can be approximated by the top layer. In this regard, it can be concluded that the strain rate increases linear with radius r in regions, where sticking of stud material to the substrate occurs. If slipping occurs, there is no dependency of the strain rate on radius r. Therefore, it can be deduced that the radius-dependent shear flow stress near the interface mainly depends on the local stud material temperature over the radius in regions were slipping occurs, which is predominantly the case in regions without deposition. The strain rate increases with radius r in those regions, where sticking occurs, i.e. material deposition takes place. As a result, the increased strain rate additionally influences the shear flow stress. Therefore, due to the slightly lower temperature at the center of the stud, a higher local shear flow stress of the stud material there, compared to the surrounding material can be assumed. Taking into account that shearing of the stud material and its adhesion to the substrate during the process only occurs when the bonding strength σ_{bond}, which is defined as the strength of the stud material to adhere with the substrate, exceeds the critical shear stress σ_f, which is the stress required for plastic material flow of the stud tip material, the local material properties during the process play a crucial role enabling deposition. Bonding conditions between successful and unsuccessful material deposition can thus be expressed via:

- material deposition by stud shearing: $\sigma_f \leq \sigma_{bond}$,
- no material deposition: $\sigma_f > \sigma_{bond}$.

The bonding strength σ_{bond} in the joining interface during the process depends on the chemical composition of the alloys used as well as on local temperatures. If only the chemical composition is taken into account and since it does not change during the FS process, the strength in the joining interface can be considered constant. However, the process temperature influences both the diffusion rate and the flow stress of the materials. Although a higher process temperature increases

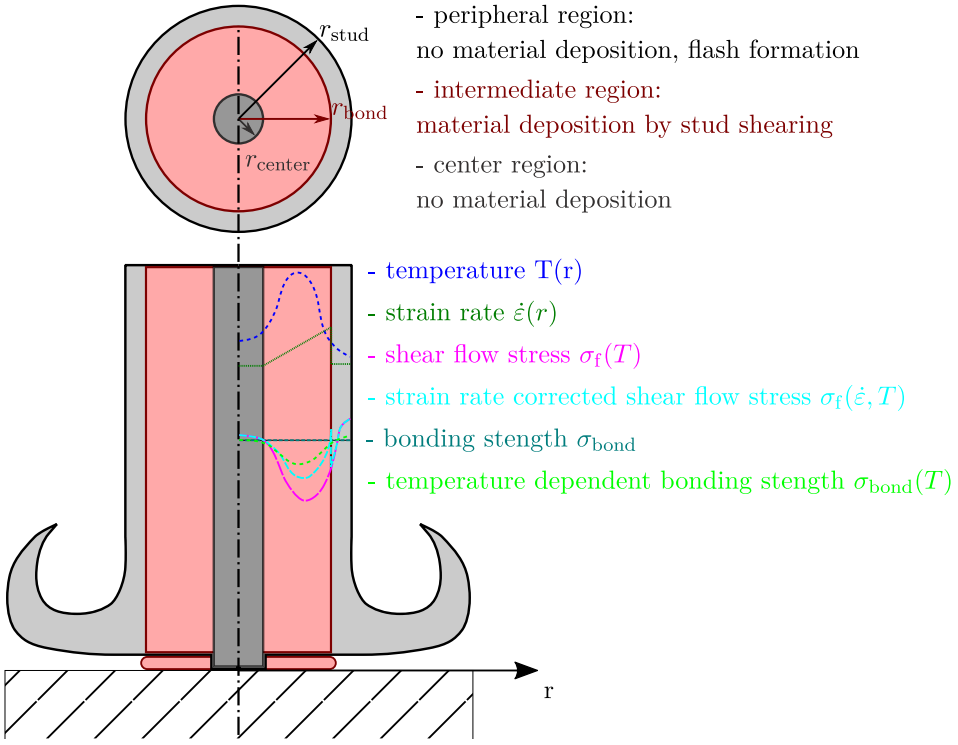

Fig. 8. Material deposition theory derived from the dissimilar FS process of aluminum alloys on Ti6Al4V.

the diffusion rate between the materials, it significantly reduces their flow stresses. Since the flow stress of the materials can be regarded as the dominant influencing factor on the bonding strength for the slow diffusion pairs in question, the resulting bonding strength for the dissimilar material combinations under consideration is expected to be low.

With the results from EBSD analysis, stop action tests and the appearances of layer and stud tip after the process, material deposition for the FS process of aluminum alloys on Ti6Al4V can be interpreted as illustrated in Fig. 8. The stud tip is divided into three sections. One section is the region in the center, defined by the radius r_{center}. Within this region, the process temperatures seem to be insufficient to soften the stud material due to the higher shear flow stress to fulfill the bonding condition and thus no bonding of stud tip material takes place during the process. The radius r_{center} mainly depends on the selected process parameters, which determine the heat input and therefore the final process temperature. Here, the stud material is in direct contact with the substrate. However, the analysis of the radius of the 'real rotational contact plane' r_c according to Eq. (1) and the measurement of the keyhole-counterpart geometries at the stud tip r_{center} reveal that the calculation of r_c seems not to be valid for dissimilar material combinations, i.e. $r_{c,6082} = 2.98$ mm vs. $r_{center,6082} = 8.10$ mm. Contrary to Fukakusa's theory, the calculation of the 'real rotational contact plane' is only valid when the material from the center of the stud is also deposited, which is not the case for dissimilar material combinations.

The second section is the intermediate region between the center and the peripheral region of the stud, which is defined as the bonding region, reaching from r_{center} to the outer radius r_{bond}. In this region, due to the hotter and therefore softer stud material, bonding can be achieved as material is sheared off the stud tip and attached to the substrate surface. This is supported by the EBSD results, which show that the layer material has a shear texture, indicating that the material is sheared from the stud tip. The texture intensities given for AA6082 are higher then the ones for AA7050. This can be explained by the fact that r_{center} is larger for AA6082. Thus, the AA7050 material is sheared off from the stud tip at an earlier stage of the process and experiences more recrystallization. In the peripheral region, the temperature decreases and thus the stud's flow stress increases there. The material from this region typically forms the flash during FS, where also for similar material combinations no material deposition occurs. Fig. 8 shows these regions and the qualitative curves of temperature, strain rate, shear flow stress and bonding strength. The present study and its theory can provide an impetus for future experimental work, especially on dissimilar material combinations such as the deposition of Al alloys on Ti substrates.

5. Conclusions

In the present study, the feasibility of the FS process for depositing the aluminum alloys AA6082 and AA7050 on the titanium alloy Ti6Al4V has been investigated. The main findings can be summarized as follows:

- The same axial force and translational speed ranges need to be applied for both alloys, but higher rotational speeds for AA6082 are required to maintain stud tip temperature due to its higher thermal conductivity and resistance to rotational movement.
- Substrate temperatures near the interface are 490.3 °C for AA6082 and 422.9 °C for AA7050, equaling 87–92% of their solidus temperatures.
- A new theory for dissimilar material deposition divides the stud tip into three zones: no deposition in the center, FS-typical flash in the periphery, and successful deposition in the intermediate zone due to higher temperatures and lower shear flow stresses.
- The kind of material deposition behavior depends on differences in stud and substrate properties, such as strength, thermal conductivity, and solidus temperature.
- FS bonding occurs through mechanical interlocking and diffusion. For AA6082 on Ti6Al4V, IMCS form, indicating diffusion, while for AA7050, no diffusion can be verified. It is mainly the process temperature that influences the bonding mechanism.

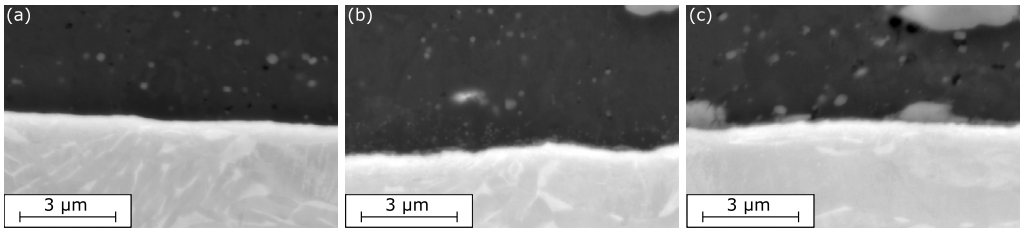

Fig. 9. Interface of AA6082-Ti6Al4V with increasing IMC thickness from the edge of the layer (a) towards the center (b, c) of the layer (Fig. 4(c, e)).

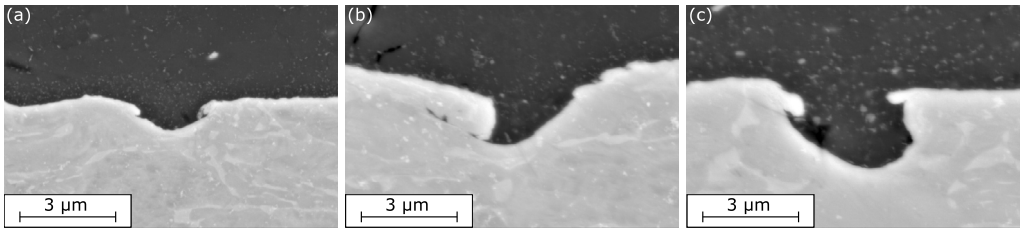

Fig. 10. Interface of AA7050-Ti6Al4V with areas indicating mechanical interlocking as part of the bonding between deposit and substrate (Fig. 4 (d, f)).

CRediT authorship contribution statement

Marius Hoffmann: Writing – review & editing, Writing – original draft, Visualization, Validation, Methodology, Investigation, Formal analysis, Data curation, Conceptualization. **Arne Roos:** Writing – review & editing, Supervision. **Benjamin Klusemann:** Writing – review & editing, Supervision, Resources, Funding acquisition, Conceptualization.

Funding

The work was carried out under the auspices of the AVAIL-DE project (project number 20W1906E), which is funded by the German Federal Ministry of Economic Affairs and Climate Action (BMWK) under the LuFo VI-1 program.

Declaration of competing interest

The authors declare that they have no known competing financial interests or personal relationships that could have appeared to influence the work reported in this paper.

Appendix A. Interface AA6082-Ti6Al4V

Fig. 9 shows the increase of the thickness of IMC layer at the interface for AA6082 deposits on Ti6Al4V. Fig. 9(a) refers to a position at the edge of the deposit where no IMC layer can be detected using SEM. Fig. 9(b, c) correspond to positions close to the center of the layer and show a IMC layer thickness between Figs. 9(a) and 4(c, e).

Appendix B. Interface AA7050-Ti6Al4V

Fig. 10 shows areas at the interface for AA7050 deposits on Ti6Al4V that indicate the mechanical interlocking as part of the bonding between the deposit and the substrate. No IMC layer can be detected in these spots.

Appendix C. Bonding mechanisms

Bonding during FS mainly takes place by mechanical interlocking and diffusion processes as described in the review by Gandra et al. [52]. Thus the bonding strength between deposit and substrate material is expected to depend on factors like the degree of mechanical interlocking, provided by a combination of the substrate surface topography and the material combination, i.e. the chemical composition of stud and substrate material, and their chemical affinity under the process temperatures as influencing factors for diffusion processes and the formation of IMCs. In numerous diffusion bonding studies, it is shown that the growth of IMCs is a sequential two stage process. In the reaction-controlled stage, IMCs are formed based on chemical reactions between Al and Ti atoms, whereas in the diffusion-controlled stage the diffusion of Al and Ti atoms control the growth of IMC layer [59]. For the Al-alloys used, differ significantly in their chemical composition and mechanical properties. Thus, differences in the formation of IMCs are revealed via SEM interface investigation, Fig. 4. Since IMCs could only be detected for AA6082 in this work using SEM, it can be concluded that either the required processing conditions for the chemical reaction between Al and Ti during the deposition of AA7050 was not sufficient or the IMC growth kinetic was too low to grow to a SEM-detectable thickness. However, using higher resolution methods can lead to different results at the AA7050-Ti6Al4V interface since it might be possible to detect smaller IMC layers, which were not detectable using SEM. For instance, reaction/diffusion kinetic between the Al and Ti alloys investigated is considered slow at the obtained process temperatures and the short processing times applied, i.e. between 10 and 20 s for the selected process parameters. Wilden and Bergmann [60] showed that for the diffusion bonding of AA6018 to Ti6Al4V, a minimum temperature of 480 °C is necessary in order to achieve a bonding with processing times below 1 h. This temperature was only exceeded for the AA6082 deposition process. By analyzing different locations at the interface for AA6082-Ti6Al4V, see Fig. 9, a decrease in thickness of the IMC can be observed towards the edge of the layer, where lower process temperatures have also been detected. The fact that in the current study the IMC layer was observable for AA6082 on Ti6Al4V only, indicates that for this material combination the contribution of diffusion to the bonding was more dominant than for AA7050 on Ti6Al4V, whereas mechanical interlocking seems to be more dominant for AA7050 on Ti6Al4V than for AA6082 layers as indicated in Fig. 10.

Data availability

Data will be made available on request.

References

[1] H. Klopstock, A.R. Neelands, An improved method of joining or welding metals, British Patent Specification 572789, 1941.

[2] J. Akram, P.R. Kalvala, M. Misra, Effect of process parameters on friction surfaced coating dimensions, Adv. Mater. Res. 922 (2014) 280–285, http://dx.doi.org/10.4028/www.scientific.net/AMR.922.280.

[3] Z. Rahmati, H.J. Aval, S. Nourouzi, R. Jamaati, Effect of friction surfacing parameters on microstructure and mechanical properties of solid-solutionized AA2024 aluminium alloy cladded on AA1050, Mater. Chem. Phys. 269 (2021) 124756, http://dx.doi.org/10.1016/j.matchemphys.2021.124756.

[4] K. Badheka, V. Badheka, Friction surfacing of aluminium on steel: An experimental approach, Mater. Today: Proc. 4 (9) (2017) 9937–9941, http://dx.doi.org/10.1016/j.matpr.2017.06.297.

[5] K.P. Rao, A. Sankar, H.K. Rafi, G.D.J. Ram, G.M. Reddy, Friction surfacing on nonferrous substrates: a feasibility study, Int. J. Adv. Manuf. Technol. 65 (5–8) (2013) 755–762, http://dx.doi.org/10.1007/s00170-012-4214-0.

[6] J. Gandra, P. Vigarinho, D. Pereira, R.M. Miranda, A. Velhinho, P. Vilaça, Wear characterization of functionally graded al–SiC composite coatings produced by friction surfacing, Mater. Des. (1980- 2015) 52 (2013) 373–383, http://dx.doi.org/10.1016/j.matdes.2013.05.059.

[7] R. Farajollahi, H.J. Aval, R. Jamaati, Effect of friction surfacing on the microstructural and wear characteristics of Al-Cu-Mg alloy coating reinforced by nickel aluminide, Intermetallics 142 (6) (2022) 107440, http://dx.doi.org/10.1016/j.intermet.2021.107440.

[8] D.K. Sahoo, S.B. Chaudhary, N. Neupane, B.H. Babu, Improving the mechanical and corrosion behaviour of friction surfaced aluminium deposition by forced convection nitrogen shielding technique, J. Inst. Eng. (India): Ser. D 698 (6) (2023) 249, http://dx.doi.org/10.1007/s40033-023-00496-5.

[9] H. Agiwal, H. Yeom, K.A. Ross, K. Sridharan, F.E. Pfefferkorn, Leak-tight crack repair for 304L stainless steel using friction surfacing, J. Manuf. Process. 79 (4) (2022) 532–543, http://dx.doi.org/10.1016/j.jmapro.2022.05.004.

[10] J. Dilip, G.D.J. Ram, Microstructure evolution in aluminum alloy AA 2014 during multi-layer friction deposition, Mater. Charact. 86 (2013) 146–151, http://dx.doi.org/10.1016/j.matchar.2013.10.009.

[11] A. Kar, S. Kumar, S.V. Kailas, Developing multi-layered 3D printed homogenized structure using solid state deposition method, Mater. Charact. 199 (6) (2023) 112770, http://dx.doi.org/10.1016/j.matchar.2023.112770.

[12] M. Hoffmann, A. Roos, B. Klusemann, Investigation of microstructural and mechanical properties in AA2024-T351 multi-layer friction surfacing, Surf. Coat. Technol. 480 (4) (2024) 130610, http://dx.doi.org/10.1016/j.surfcoat.2024.130610.

[13] H. Agiwal, C. Baumann, S. Krall, H. Yeom, K. Sridharan, F. Bleicher, F.E. Pfefferkorn, Towards multilayered coatings of 304L stainless steels using friction surfacing, J. Manuf. Sci. Eng. 145 (1) (2023) 1062, http://dx.doi.org/10.1115/1.4055050.

[14] S. Sambasivam, N. Gupta, Ali Saeed Jassim, D. Pratap Singh, S. Kumar, J. Mohan Giri, M. Gupta, A review paper of FSW on dissimilar materials using aluminum, Mater. Today: Proc. (2023) http://dx.doi.org/10.1016/j.matpr.2023.03.304.

[15] V.S. Gadakh, V.J. Badheka, A.S. Mulay, Solid-state joining of aluminum to titanium: A review, Proc. Inst. Mech. Eng. L: J. Mater.: Des. Appl. 235 (8) (2021) 1757–1799, http://dx.doi.org/10.1177/14644207211010839.

[16] W.V. Vaidya, M. Horstmann, V. Ventzke, B. Petrovski, M. Koçak, R. Kocik, G. Tempus, Improving interfacial properties of a laser beam welded dissimilar joint of aluminium AA6056 and titanium Ti6Al4V for aeronautical applications, J. Mater. Sci. 45 (22) (2010) 6242–6254, http://dx.doi.org/10.1007/s10853-010-4719-6.

[17] S. Kuryntsev, A review: Laser welding of dissimilar materials (Al/Fe, Al/Ti, Al/Cu)-methods and techniques, microstructure and properties, Mater. (Basel, Switz.) 15 (1) (2021) http://dx.doi.org/10.3390/ma15010122.

[18] K.-S. Bang, K.-J. Lee, H.-S. Bang, H.-S. Bang, Interfacial microstructure and mechanical properties of dissimilar friction stir welds between 6061-T6 aluminum and Ti-6%Al-4%V alloys, Mater. Trans. 52 (5) (2011) 974–978, http://dx.doi.org/10.2320/matertrans.L-MZ201114.

[19] X. Meng, Y. Xie, S. Sun, X. Ma, L. Wan, J. Cao, Y. Huang, Lightweight design: Friction-based welding between metal and polymer, Acta Met. Sin. (Engl. Lett.) 36 (6) (2023) 881–898, http://dx.doi.org/10.1007/s40195-023-01552-5.

[20] A. Kar, S.V. Kailas, S. Suwas, Formation sequence of intermetallics and kinetics of reaction layer growth during solid state reaction between titanium and aluminum, Materialia 11 (4) (2020) 100702, http://dx.doi.org/10.1016/j.mtla.2020.100702.

[21] Y.-C. Kim, A. Fuji, Factors dominating joint characteristics in Ti – Al friction welds, Sci. Technol. Weld. Join. 7 (3) (2002) 149–154, http://dx.doi.org/10.1179/136217102225004185.

[22] M. Aonuma, K. Nakata, Dissimilar metal joining of 2024 and 7075 aluminium alloys to titanium alloys by friction stir welding, Mater. Trans. 52 (5) (2011) 948–952, http://dx.doi.org/10.2320/matertrans.L-MZ201102.

[23] A. Kar, S.V. Kailas, S. Suwas, Friction stir welding of aluminum to titanium: quest for optimum tool-offset, deformation of titanium, and mechanism of joint formation, Int. J. Adv. Manuf. Technol. 128 (5–6) (2023) 1943–1956, http://dx.doi.org/10.1007/s00170-023-12065-x.

[24] Y. Huang, Z. Lv, L. Wan, J. Shen, J.F. dos Santos, A new method of hybrid friction stir welding assisted by friction surfacing for joining dissimilar Ti/Al alloy, Mater. Lett. 207 (2017) 172–175, http://dx.doi.org/10.1016/j.matlet.2017.07.081.

[25] L. Zhou, M. Yu, B. Liu, Z. Zhang, S. Liu, X. Song, H. Zhao, Microstructure and mechanical properties of al/steel dissimilar welds fabricated by friction surfacing assisted friction stir lap welding, J. Mater. Res. Technol. 9 (1) (2020) 212–221, http://dx.doi.org/10.1016/j.jmrt.2019.10.046.

[26] I. Esther, I. Dinaharan, N. Murugan, Microstructure and wear characterization of AA2124/4wt.%B4C nano-composite coating on Ti–6Al–4V alloy using friction surfacing, Trans. Nonferr. Met. Soc. China 29 (6) (2019) 1263–1274, http://dx.doi.org/10.1016/S1003-6326(19)65033-8.

[27] G.M. Reddy, K.S. Prasad, K.S. Rao, T. Mohandas, Friction surfacing of titanium alloy with aluminium metal matrix composite, Surf. Eng. 27 (2) (2011) 92–98, http://dx.doi.org/10.1179/174329409X451128.

[28] K. Fukakusa, On the characteristics of the rotational contact plane – a fundamental study of friction surfacing, Weld. Int. 10 (7) (1996) 524–529, http://dx.doi.org/10.1080/09507119609549043.

[29] M. Hoffmann, Z. Kallien, E. Antunes Duda, B. Klusemann, Insight into layer formation during friction surfacing: Relationship between deposition behavior and microstructure, Mater. Today Commun. 41 (2) (2024) 110337, http://dx.doi.org/10.1016/j.mtcomm.2024.110337.

[30] H.K. Rafi, G. Phanikumar, K.P. Rao, Material flow visualization during friction surfacing, Met. Mater. Trans. A 42 (4) (2011) 937–939, http://dx.doi.org/10.1007/s11661-011-0614-2.

[31] C. Belei, V. Fitseva, J.F. dos Santos, N.G. Alcântara, S. Hanke, Tic particle reinforced Ti-6Al-4V friction surfacing coatings, Surf. Coat. Technol. 329 (2017) 163–173, http://dx.doi.org/10.1016/j.surfcoat.2017.09.050.

[32] X.M. Liu, Z.D. Zou, Y.H. Zhang, S.Y. Qu, X.H. Wang, Transferring mechanism of the coating rod in friction surfacing, Surf. Coat. Technol. 202 (9) (2008) 1889–1894, http://dx.doi.org/10.1016/j.surfcoat.2007.08.024.

[33] H.K. Rafi, G.J. Ram, G. Phanikumar, K.P. Rao, Friction surfaced tool steel (H13) coatings on low carbon steel: A study on the effects of process parameters on coating characteristics and integrity, Surf. Coat. Technol. 205 (1) (2010) 232–242, http://dx.doi.org/10.1016/j.surfcoat.2010.06.052.

[34] K.P. Rao, A. Veera Sreenu, H.K. Rafi, M.N. Libin, K. Balasubramaniam, Tool steel and copper coatings by friction surfacing – a thermography study, J. Mater. Process. Technol. 212 (2) (2012) 402–407, http://dx.doi.org/10.1016/j.jmatprotec.2011.09.023.

[35] M.M. da Silva, M.L.B. Afonso, S.L.N. Silva, F.C.T.D. Troysi, Í.B. dos Santos, P.P. Brito, Application of the friction surfacing process in a CNC machining center: a viability assessment for producing al-alloy coatings on low carbon steel, J. Braz. Soc. Mech. Sci. Eng. 40 (1) (2018) 1062, http://dx.doi.org/10.1007/s40430-017-0947-x.

[36] DIN EN 573-3:2019-10, Aluminium and aluminium alloys - chemical composition and form of wrought products - part 3: Chemical composition and form of products, 2019.

[37] ASTM, B265, Standard specification for titanium and titanium alloy strip, sheet, and plate, 2020.

[38] V. Fitseva, H. Krohn, S. Hanke, J.F. dos Santos, Friction surfacing of Ti–6Al–4V: Process characteristics and deposition behaviour at various rotational speeds, Surf. Coat. Technol. 278 (2015) 56–63, http://dx.doi.org/10.1016/j.surfcoat.2015.07.039.

[39] J. Gandra, D. Pereira, R.M. Miranda, P. Vilaça, Influence of process parameters in the friction surfacing of AA 6082-T6 over AA 2024-T3, Procedia CIRP 7 (2013) 341–346, http://dx.doi.org/10.1016/j.procir.2013.05.058.

[40] H. Li, W. Qin, A. Galloway, A. Toumpis, Friction surfacing of aluminium alloy 5083 on DH36 steel plate, Metals 9 (4) (2019) 479, http://dx.doi.org/10.3390/met9040479.

[41] D. Sahoo, B. Mohanty, A. Maalika Veetil, Evaluation of bond strength and flash mass on friction surfaced deposition of aluminium 6063 over IS 2062 low carbon steel using different mechtrode face, Ann. Chim. - Sci. Mater. 44 (2) (2020) 109–119, http://dx.doi.org/10.18280/acsm.440206.

[42] D.K. Sahoo, B. Sundar Mohanty, A.M. Pradeep, A. David Feby John, An experimental study on friction surfaced coating of aluminium 6063 over AISI 316 stainless steel substrate, Mater. Today: Proc. 40 (2) (2021) S10–S18, http://dx.doi.org/10.1016/j.matpr.2020.03.251.

[43] A. Singh, V. Upadhyay, Mechanical and microstructural behavior of similar and dissimilar AA6082-T6 and AA7050-T7 friction stir welded joints, J. Inst. Eng. (India): Ser. D 103 (1) (2022) 225–234, http://dx.doi.org/10.1007/s40033-022-00338-w.

[44] Y. Zhang, Z. Ren, J. Ju, Z. Liu, A coupled acoustic-thermal-fluid model and numerical simulation of ultrasound vibration assisted friction surfacing, Sci. Technol. Weld. Join. 25 (2) (2020) 135–141, http://dx.doi.org/10.1080/13621718.2019.1645375.
[45] T. Luijendijk, Welding of dissimilar aluminium alloys, J. Mater. Process. Technol. 103 (1) (2000) 29–35, http://dx.doi.org/10.1016/S0924-0136(00)00415-5.
[46] T.-J. Bian, H. Li, C. Lei, C.-H. Wu, L.-W. Zhang, Microstructures and properties evolution of Al-Zn-Mg-Cu alloy under electrical pulse assisted creep aging, Adv. Manuf. 10 (4) (2022) 596–609, http://dx.doi.org/10.1007/s40436-022-00404-2.
[47] M. Reimann, Keyhole Repair in Precipitation Hardening Aluminum Alloys using Refill Friction Stir Spot Welding (Ph.D. thesis), TUHH Universitätsbibliothek, Hamburg, 2018, http://dx.doi.org/10.15480/882.1878.
[48] L. Djapic Oosterkamp, A. Ivankovic, G. Venizelos, High strain rate properties of selected aluminium alloys, Mater. Sci. Eng.: A 278 (1–2) (2000) 225–235, http://dx.doi.org/10.1016/S0921-5093(99)00570-5.
[49] Jiang Li, Fuguo Li, Jun Cai, Ruiting Wang, Zhanwei Yuan, Fengmei Xue, Flow behavior modeling of the 7050 aluminum alloy at elevated temperatures considering the compensation of strain, Mater. Des. 42 (2012) 369–377, http://dx.doi.org/10.1016/j.matdes.2012.06.032.
[50] M. Schikorra, L. Donati, L. Tomesani, A. Tekkaya, Microstructure analysis of aluminum extrusion: Grain size distribution in AA6060, AA6082 and AA7075 alloys, J. Mech. Sci. Technol. 21 (2007) 1445–1451, http://dx.doi.org/10.1007/BF03177357.
[51] F. Krumphals, P. Sherstnev, S. Mitsche, S. Randjelovic, C. Sommitsch, Physically based microstructure modelling of AA6082 during hot extrusion, Key Eng. Mater. 424 (2009) 27–34, http://dx.doi.org/10.4028/www.scientific.net/kem.424.27, Trans Tech Publications, Ltd.
[52] J. Gandra, H. Krohn, R.M. Miranda, P. Vilaça, L. Quintino, J.F. dos Santos, Friction surfacing—A review, J. Mater. Process. Technol. 214 (5) (2014) 1062–1093, http://dx.doi.org/10.1016/j.jmatprotec.2013.12.008.
[53] Z. Kallien, B. Klusemann, Combined experimental-numerical analysis of the temperature evolution and distribution during friction surfacing, Surf. Coat. Technol. 437 (8) (2022) 128350, http://dx.doi.org/10.1016/j.surfcoat.2022.128350.
[54] Z. Kallien, L. Rath, A. Roos, B. Klusemann, Experimentally established correlation of friction surfacing process temperature and deposit geometry, Surf. Coat. Technol. 397 (6) (2020) 126040, http://dx.doi.org/10.1016/j.surfcoat.2020.126040.
[55] Q. Yang, X. Liu, Y. Liu, X. Fan, M. Shu, The flow softening behavior and deformation mechanism of AA7050 aluminum alloy, Mater. Trans. 60 (9) (2019) 2041–2047, http://dx.doi.org/10.2320/matertrans.MT-M2019114.
[56] H. Wang, P.A. Colegrove, H.M. Mayer, L. Campbell, J.D. Robson, Material constitutive behaviour and microstructure study on aluminium alloys for friction stir welding, Adv. Mater. Res. 89–91 (2010) 615–620, http://dx.doi.org/10.4028/www.scientific.net/AMR.89-91.615.
[57] P. Rai, S.C.J. Daniel, R. Damodaram, D. Yadav, Microstructural characterization, mechanical properties and thermal stability of friction surfaced inconel 718 coatings, Met. Mater. Trans. A 214 (3) (2023) 1062, http://dx.doi.org/10.1007/s11661-023-07031-x.
[58] P. Pirhayati, H.J. Aval, Phase-field microstructure simulation during aluminum alloy friction surfacing, Surf. Coat. Technol. 402 (2020) 126496, http://dx.doi.org/10.1016/j.surfcoat.2020.126496.
[59] N. Thiyaneshwaran, K. Sivaprasad, B. Ravisankar, Characterization based analysis on TiAl3 intermetallic phase layer growth phenomenon and kinetics in diffusion bonded Ti/TiAl3/Al laminates, Mater. Charact. 174 (1) (2021) 110981, http://dx.doi.org/10.1016/j.matchar.2021.110981.
[60] J. Wilden, J.P. Bergmann, Manufacturing of titanium/aluminium and titanium/steel joints by means of diffusion welding, Weld. Cut. 3 (5) (2004) 285–290.